Photophysics of Xanthene Dyes at High Concentrations in Solid Environments: Charge Transfer Assisted Triplet Formation

*Yair E. Litman,[1,§] Hernán B. Rodríguez,[2] Silvia E. Braslavsky,[1,3] and Enrique San Román[1]**

[1] Universidad de Buenos Aires. Consejo Nacional de lnvestigaciones Cientificas y Tecnicas. Instituto de Química Física de los Materiales, Medio Ambiente y Energía (INQUIMAE). Facultad de Ciencias Exactas y Naturales, Ciudad Universitaria, Pab. II, Buenos Aires, Argentina

[2] Instituto de Investigaciones Fisicoquímicas Teóricas y Aplicadas (INIFTA), CCT-La Plata-CONICET, Universidad Nacional de La Plata (UNLP), Diag. 113 y Calle 64, La Plata, Argentina

[3] Max Planck Institute for Chemical Energy Conversion, Stiftstrasse 34-36, 45410 Mülheim an der Ruhr, Germany

* E-mail: esr@qi.fcen.uba.ar, Tel. +5411-4576-3378 Ext. 118, Fax +5411-4576-3341

[§] Present address: Fritz Haber Institute of the Max Planck Society, Faradayweg 4–6, 14195 Berlin, Germany

ABSTRACT

The photophysical behavior of two xanthene dyes, Eosin Y and Phloxine B, included in microcrystalline cellulose particles is studied in a wide concentration range, with emphasis on the effect of dye concentration on fluorescence and triplet quantum yields. Absolute fluorescence quantum yields in the solid-state were determined by means of diffuse reflectance and steady-state fluorescence measurements, while absolute triplet quantum yields were obtained by laser-induced optoacoustic spectroscopy and their dependence on dye concentration was confirmed by diffuse reflectance laser flash photolysis and time-resolved phosphorescence measurements. When both quantum yields are corrected for reabsorption and reemission of radiation, Φ_F values decrease strongly on increasing dye concentration, while a less pronounced decay is observed for Φ_T. Fluorescence concentration quenching is attributed to the formation of dye aggregates or virtual traps resulting from molecular crowding. Dimeric traps are however able to generate triplet states. A mechanism based on the intermediacy of charge-transfer states is proposed and discussed. Calculation of parameters for photoinduced electron transfer between dye molecules within the traps evidences the feasibility of the proposed mechanism. Results demonstrate that photoactive energy traps, capable of yielding dye triplet states, can be formed even in highly-concentrated systems with random dye distributions.

KEYWORDS

Xanthene dyes, microcrystalline cellulose, fluorescence, triplet state, charge-transfer

INTRODUCTION

Results concerning the formulation of photoactive materials obtained by our research group during the last years show that concentration quenching (CQ) precludes the achievement of efficient materials at not quite high dye concentrations. In particular, for xanthenes and similar dyes, we demonstrated that, even in the absence of spectroscopically detectable aggregation, dye pairs with molecules separated by less than 1.5 nm behave as virtual traps for the excitation energy (1). Beddard and Porter concluded long ago that, to prevent trap formation by orbital overlap, the minimum distance between chlorophyll molecules should be 1 nm when averaged over all orientations at random (2). Thus, even if interactions do not lead to the formation of stable ground state dimers, when dyes are distributed at random over a solid volume, their effective concentration should be lower than 5 mM for CQ to be ineffective (3,4). In the recent literature, this effect is usually referred to as aggregation-caused quenching (ACQ) but it is preferable to preserve this terminology to the cases in which stable ground state aggregates are formed.

The effect of concentration on the photophysical properties of dyes has been addressed in the fifties (5-6) but it ~~concealed~~ attracted recently renewed attention, leading to the discovery of effects which, in contrast to CQ, favor emission at high concentrations. Among them aggregation induced emission (AIE) or aggregation induced emission enhancement (AIEE) (7), crystallization induced emission (CIE) or crystallization induced emission enhancement (CIEE) (8), and related phenomena (9) can be cited. Even, aggregation induced intersystem crossing (AI-ISC) arising from matching of singlet and triplet energies on aggregation has been reported (10).

Conventional dyes like xanthenes, prototypical molecules showing CQ, undergo π-π stacking both in solution of poor solvents and in the solid state. Other molecules, generally showing crowded phenyl substitution like tetraphenylethylene, suffer from rapid internal conversion owing to coupling of the electronic wave function to phenyl twisting or internal rotation, which is hindered upon aggregation, in the solid state or through binding to other molecules, leading to AIE (11). We demonstrated that a fluorescein derivative, the neutral form of 9-[1-(2-Methyl-4-methoxyphenyl)]-6-hydroxy-3H-xanthen-3-one, enhances its fluorescence quantum yield, Φ_F = 0.01 in water, nearly 30 times when included into microcrystalline cellulose (12). Immobilization of the phenyl group of the dye may be responsible for this behavior, though inhibition of intramolecular charge transfer leading to de-excitation cannot be ruled out in this case owing to the low polarity of cellulose. Applications like optoelectronics, chemosensing and biological probes would benefit from the above-mentioned fluorescence enhancing effects.

Charge transfer cannot be excluded at short distances between chemically linked species or independent molecules brought together at high concentrations. Under appropriate conditions, geminate radical anion – radical cation recombination may lead to the formation of dye triplet states, as it has been found in the reaction center of photosystem II. The $^1(P680^+Ph^-)$ (Ph: pheophytin) radical pair formed by excitation of P680 and subsequent electron transfer to Ph reverts to $^3(P680^+Ph^-)$, decaying finally to the P680 triplet state. Energy transfer from the triplet radical pair to molecular oxygen has been recognized as an important source of $^1O_2$ in photosynthesis (13). The same mechanism has been also reported in solution involving different moieties of the same molecule (14) and under aggregation of different dyes (15). In the context of photovoltaic materials this reaction pathway represents an important ~~efficiency loss~~ channel leading to efficiency loss and efforts have been made in order to suppress it (16, 17).

Previous studies were carried out by us on the photophysics of two xanthene dyes, Eosin Y (EoY) (18) and Phloxine B (PhB) (19) included into microcrystalline cellulose particles (see structures in Scheme I). The concentration dependence of their absorption and fluorescence spectra was studied, their aggregation tendency was analyzed and the decay of singlet and triplet states was investigated. It is worth noting that in this matrix the dyes are protected from quenching by molecular oxygen due to the highly reduced mobility of this species in dry cellulose (20), allowing the study of triplet states without the need of degassing. In the present work, we present a natural continuation of those studies, focusing on the effect of dye concentration on fluorescence and triplet quantum yields. We apply a battery of complementary techniques and show that generation of triplet states due to charge recombination is possible at concentrations at which CQ prevents fluorescent emission ~~and~~. We also explain the reasons ~~of~~ for this behavior. This finding is relevant if photosensitization reactions involving the triplet state are the target objective.

Scheme I

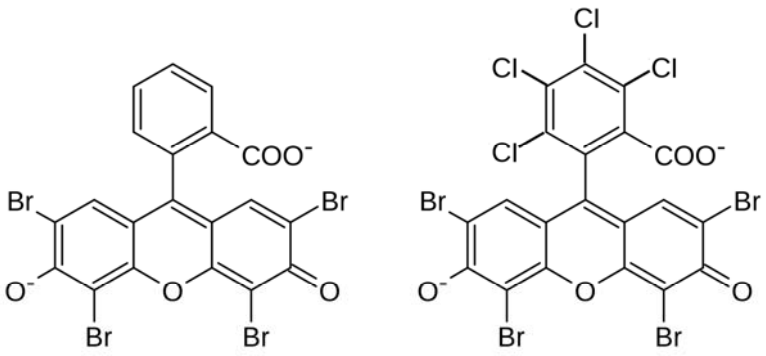

Eosin Y Phloxine B

MATERIALS AND METHODS

Materials and sample preparation. EoY disodium salt (90%), PhB (89%), and Brilliant Blue G (BBG, pure), used as calorimetric reference for laser-induced optoacoustic spectroscopy (LIOAS) measurements, were purchased from Sigma-Aldrich and used without further purification. Dye purity was checked spectroscopically. Ethanol (Cicarelli, ACS grade) and microcrystalline cellulose powder (Aldrich, pH 5-7, average particle size 20 μm) were also used as received.

Dyed-cellulose samples were prepared by suspending weighed amounts of cellulose (1.5 g, previously dried under vacuum at 40 °C during 48 h) in dye stock solutions (30 cm^3) in ethanol. The suspensions were shaken for 5 minutes, the solvent evaporated at low pressure in a rotavap at 40°C, adjusting vacuum to attain total solvent evaporation in ca. 15 minutes, and the solids were dried in a vacuum at 40°C for 48 h and maintained in the dark. Samples spanned two orders of magnitude in dye concentration, from ca. 0.04 to 5 μmol dye/g microcrystalline cellulose. All measurements were performed at room temperature on optically thick and thin layers of particles. A layer depth of 0.2 cm ensures optical thickness (no light transmission). Optically thick layers were prepared by packing the samples into a suitable holder with a Plexiglas stab, releasing pressure before measurements. Thin layers were prepared by spreading a small amount of the sample on a double-sided sticky tape fixed to a glass support.

Reflectance and emission measurements. Total and diffuse reflectance spectra of optically thick solid layers were measured in a Shimadzu UV-3600 scanning spectrophotometer equipped with an integrating sphere, using barium sulfate as the 100% reflectance reference. As samples are in general highly fluorescent, reflectance spectra are strongly distorted. Therefore, the procedure reported in ref. (21) was used. Accordingly, reflectance spectra were obtained with and without a suitable optical filter, BG38 (Schott, 0.2 cm thickness), placed before the detector located below

the integrating sphere, capable of absorbing a substantial fraction of the fluorescence. This procedure allows the absolute determination of observed fluorescence quantum yields ($\Phi_{F,obs}$) together with true reflectance spectra. These quantum yields are affected by reabsorption and reemission of fluorescence (see below). Remission function spectra were calculated from true diffuse reflectances, R, as $F(R) = (1 - R)^2 / 2R$ (22).

Steady-state emission spectra ($\lambda_{exc.}$ = 500-505 nm) of optically thick layers were recorded on a PTI model QM-4 spectrofluorometer. Measurements were performed in front face, placing an optical filter, OG530 (Schott, 0.2 cm thickness), in front of the emission monochromator to block excitation light. All spectra were corrected according to the dependence of the detection channel responsivity on wavelength (obtained from the manufacturer and checked in our laboratory) and considering filter transmittance. Emission spectra of optically thick layers show distortions due to fluorescence reabsorption and reemission. In order to obtain fluorescence spectra devoid of these effects, front face emission measurements were also performed on thin layers of particles. For that sake, a small amount of the solid was spread on a sticky-tape and the excess of material was scraped until a constant shape in the emission spectra was attained.

LIOAS measurement of triplet quantum yields. To determine observed triplet quantum yields ($\Phi_{T,obs}$), LIOAS measurements were performed on optically thick layers containing the dyes under study and compared with those on BBG, used as a calorimetric reference, included in microcrystalline cellulose at different concentrations (23). To ensure reproducibility, optically thick layers were prepared in this case loading a specially designed aluminum holder with 60 mg of dry solid, pressing with 25.5 bar for 120 s and allowing relaxation in a desiccator at atmospheric pressure for 24 h. This procedure renders a probe with a diameter of 1 cm and a thickness of 0.2 cm. The LIOAS setup used was described in detail elsewhere (24). The probe

was excited from above with a pulsed Nd-YAG laser (Spectron, 8 ns @ 532 nm). A set of three IR filters (Schott KG5, 0.2 cm thickness) was used to avoid unwanted heating and spurious LIOAS signals, while a gray wedge filter was used to obtain variable excitation energies from 30 to 130 μJ. Using the protocol described in the previous reference, LIOAS signals are reproducible within ±10%. The energy of the laser pulse exciting the sample was measured using a Lab Master (Coherent, Ultima, Mod LM-P2) energy meter. Observed triplet quantum yields are affected by reabsorption and reemission of fluorescence, similar to $\Phi_{F,obs}$. This point will be addressed later.

Diffuse reflectance laser flash-photolysis (DRLFP) and laser-induced luminescence (LIL). These experiments were performed using the same laser employed for LIOAS measurements in order to obtain independent, although relative, measurements of observed triplet quantum yields, $\Phi_{T,obs}$. Optically thick layers were placed in a diffuse reflectance accessory inside a LP920 laser flash photolysis compartment (Edinburgh Instruments). Phosphorescence was detected by LIL measurements. For DRLFP measurements, a horizontally driven Xe lamp (Osram XBO 150 W/1 OFR) produced the analysis beam. Phosphorescence (LIL) or diffusely reflected light (DRLFP) were focused onto the slit of a computer controlled high throughput 1/4 m f/2.5 monochromator (Sciencetech 9055F) with dual 1200 l/mm diffraction gratings blazed at 450 and 700 nm. The output beam was detected on a PMT (Hamamatsu R929). According to ref. (25), for small reflectance changes the number of triplet molecules detected by DRLFP is proportional to R_0 / [$R_0 - R(t)$], where R_0 is the reflectance before the laser pulse and $R(t)$ is the reflectance at time t after the pulse. Reflectances are proportional to the voltage across the PMT anode.

Cut-off filters were placed in DRLFP measurements in front of the sample to block wavelengths of the analysis beam below 400 nm in order to avoid sample degradation and, in

both kinds of measurements, between the sample and the detector to block reflected laser light. Before exciting the samples, the laser beam was passed through different filters and solutions of BBG in ethanol in order to obtain the desired excitation energies, in the range from 2 to 400 μJ for DRLFP and from 5 to 50 μJ for LIL experiments. The excitation energy was measured with the same energy meter as before. The laser fluence at the sample surface was calculated considering a spot area of 0.14 cm^2. The DRLFP or LIL signals extrapolated to $t = 0$ were plotted as a function of the laser energy and the slope at the origin was calculated. The ratio of this value to the fraction of absorbed excitation light is proportional to $\Phi_{T,obs}$, Only relative triplet quantum yields are obtained as the proportionality constant is unknown. For principles and details see ref. (26). The setup allows the detection of triplet-triplet absorption between 600 and 700 nm and phosphorescence between 650 and 750 nm. The sharp decrease of the PMT responsivity at longer wavelengths prevented full spectral characterization. Furthermore, analysis wavelengths for studying the corresponding signals as a function of the laser energy were selected considering the compromise between signal-to-noise ratio, interference of the laser beam and sample degradation. In all cases, 64 traces were averaged. The possibility of a small contribution of phosphorescence to the DRLFP signal was taken into account (see below).

Correction of quantum yields for reabsorption and reemission. The determination of quantum yields described so far involves the quotient between the number of photons emerging (fluorescence) or triplet molecules formed and the number of photons absorbed by the sample, i.e., a technical or experimentally observed quantity ($\Phi_{F,obs}$ or $\Phi_{T,obs}$). Fluorescence reabsorption and reemission, particularly relevant at high dye concentrations for overlapping absorption and emission spectra, generally obscures the evaluation of other CQ mechanisms. In the case of fluorescence, reabsorption and reemission cause distortions in emission spectra and reduces the

total emission intensity emerging from the sample, thus leading to ~~quantum yields lower than the true~~lower fluorescence quantum yields. On the other hand, reabsorption injects fluorescence back into the system, favoring the population of triplet states, and therefore, increasing $\Phi_{T,obs}$ ~~with respect to its true value~~. Correction of quantum yields by reabsorption and reemission is therefore mandatory to evaluate the effects of dye concentration.

As reported in refs. (27-28), corrected ~~(or true)~~ fluorescence quantum yields, Φ_F, can be calculated as:

$$\Phi_F = \frac{\Phi_{F,obs}}{\alpha_0(1-P) + \Phi_{F,obs}P_\alpha} \quad (1)$$

where α_0 is the fraction of the excitation light absorbed by the dye, and P and P_α are the probabilities of fluorescence reabsorption by all the constituents in the sample and the dye, respectively ($P_\alpha = P$ if the dye is the only absorber). These parameters can be calculated from reflectance and emission data, considering any residual absorption by cellulose. Following similar arguments as used for the derivation of Eq. (1), corrected ~~(or true)~~ triplet quantum yields, Φ_T, can be calculated as:

$$\Phi_T = \frac{\Phi_{T,obs}\left(1-\Phi_F P_\alpha\right)}{\alpha_0} \quad (2)$$

The essentials of the correction methods and their applicability to light scattering solid samples, such as dyed cellulose, were reviewed elsewhere (29).

Results and Discussion

Remission function and fluorescence spectra of optically thick layers are shown for selected samples in Figure 1. The complete set of spectra, with the exception of remission function spectra for the most dilute samples, which are too noisy, are given in the Supporting Information (Figures S1a and S1b). Remission functions were calculated from true – corrected for fluorescence – diffuse reflectances (see Materials and Methods). Absorption maxima were located at (531 ± 2) and (548 ± 1) nm for EoY and PhB, respectively. Within experimental error, very small changes in spectral shape and linearity of $F(R)$ with dye concentration were observed for EoY in the whole concentration range, while noticeable changes in the ratio of band maxima and marked hypochromism (see Figure S2 in the SI) are observed for the most concentrated PhB samples. These spectral changes point to PhB dye-to-dye interactions in the ground state caused by molecular crowding at the highest concentrations, while interactions are much weaker for EoY. In a previous work (19), similar spectral changes on increasing dye concentration were found for PhB included in microcrystalline cellulose, but no hypochromism was found in that case in a similar concentration range. The difference can be ascribed to the sample preparation procedure, particularly in the solvent evaporation step (see Materials and Methods). While in the mentioned work the samples were dried overnight (at least 24 h) by slow evaporation, in the present case a rapid evaporation of the solvent (ca. 15 min) in a rotavap system was used. Considering that the swelling of cellulose in the solvent (ethanol) depends on time, a rapid evaporation precludes deep penetration of the dye, leading to dye molecular crowding at the surface of cellulose.

Fluorescence spectra of EoY and PhB at the lowest concentration show maxima at (559 ± 1) and (576 ± 1) nm, respectively. Accordingly, both dyes show similar Stokes shifts of around 28 nm (~~equivalent to~~i.e. 943 cm^{-1} for EoY and 887 cm^{-1} for PhB). A pronounced shoulder is observed for PhB. Spectra show marked changes with concentration, which are compatible with fluorescence reabsorption: red shift (both dyes) and growing of the shoulder relative to the main maximum (for PhB) on increasing concentration.

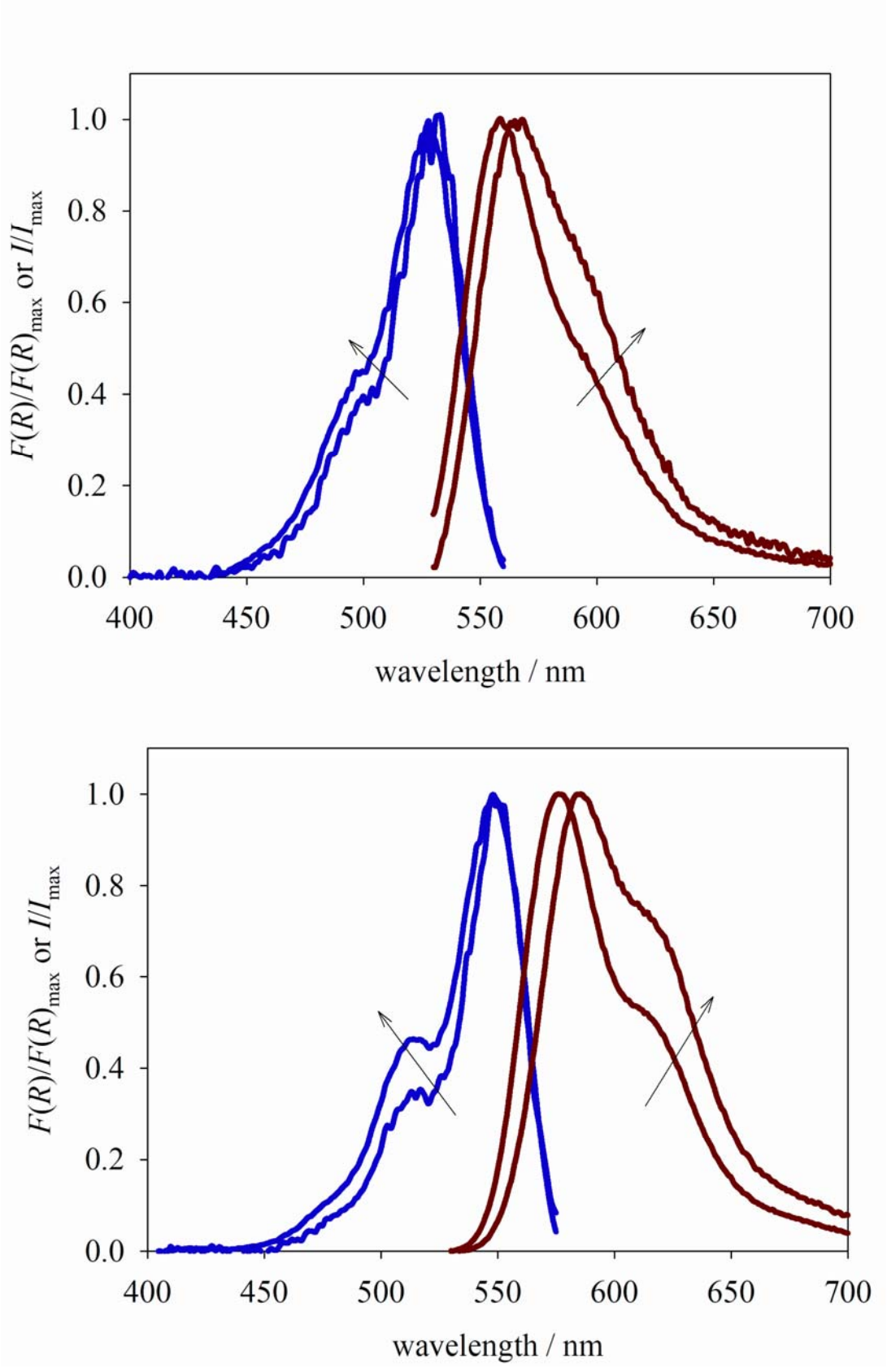
1.0
0.8
0.6
0.4
0.2
0.0
F(R)/F(R)max or I/Imax
400
450
500
550
600
650
700
wavelength / nm
1.0
0.8
0.6
0.4
0.2
0.0
F(R)/F(R)max or I/Imax
400
450
500
550
600
650
700
wavelength / nm

Figure 1. Absorption (blue) and emission (red) spectra of selected samples of EoY (upper panel, λ_{ex} = 505 nm) and PhB (lower panel, λ_{ex} = 500 nm). Dye concentrations are 0.16 and 4.2 μmol g^{-1} for both dyes. Arrows show increasing concentrations. EoY data was adapted with permission from ~~(23)~~ref. 18.

Normalized fluorescence spectra of thin layers of particles are shown in the SI (Figures S3a and S3b). For both dyes, below ca. 2 μmol g^{-1} thin layer spectra are coincident with thick layer spectra corrected by reabsorption. See for example Figure S4 in the SI. Even at concentrations for which reabsorption is negligible, red shifts still persist on increasing dye concentration. Concentration-dependent Stokes shifts, found generally in dyed materials at high concentrations, are attributed to long-range interactions (at distances higher than 10 nm) between excited dye molecules and neighboring molecules in the ground state (29). At the highest concentrations, spectra are still affected by reabsorption, though to a lesser extent than for thick layers.

In summary, for EoY remission functions at maximum are proportional to the concentration of the dye and only light changes in the shoulder at lower wavelengths are observed at the highest concentrations, pointing to very small ground-state interactions in the whole concentration range. The tendency to form aggregates is somewhat higher for PhB. Aside from variable Stokes shifts leading to the displacement of fluorescence maxima to the red as concentration increases, both dyes show similar fluorescence spectra at all concentrations. In other words, no distinct fluorescence features are observed at the highest concentrations. Absorption and corrected fluorescence spectra for both dyes in cellulose, aside from a small red-shift, resemble those of the dianionic form of the dyes in basic ethanol (3, 30).

Absolute fluorescence quantum yields were obtained from reflectance spectra (see Materials and Methods). $\Phi_{F,obs}$ and Φ_F values found for EoY and PhB are quoted in the SI (Table S2). As

Φ_F is lower than one, fluorescence reemitted in successive reabsorption-reemission steps does not compensate the loss produced by radiationless decay. As a consequence, $\Phi_{F,obs}$ decreases with concentration. On correction for reabsorption and reemission, an increase up to 35 % for EoY and 30 % for PhB is obtained at the highest concentrations but a strong decrease persists. The correction is obtained ~~by~~ using Eq. 1, ~~in which~~whose relevant parameters can be ~~obtained~~ calculated from absorption and emission spectra. Values corrected for reabsorption and reemission are shown in Figure 2 for both dyes as a function of dye concentration. Results may be fitted by a simple exponential, $\Phi_F = \Phi_{F0} \exp(-[dye]/c)$, where Φ_{F0} is the quantum yield at [dye] = 0. This function, though not bearing any physical meaning, allows extrapolation at infinite dilution and an empirical characterization of the fall off region. Parameters found are Φ_{F0} = 0.70 and c = 1.43 μmol g^{-1} for EoY and Φ_{F0} = 0.82 and c = 1.05 μmol g^{-1} for PhB. The values of Φ_F found in basic ethanol, where the dyes remain dianionic, are 0.68 for EoY (30) and 0.76 for PhB (3). For xanthene dyes, Φ_F values expected in cellulose have to be somewhat larger than those found in alcohols (23). Therefore, the experimental values found for Φ_{F0} seem to be reasonable. The method used to obtain fluorescence quantum yields from reflectance spectra yields $\Phi_{F,obs}$ and Φ_F as a function of the excitation wavelength. Error bars quoted in Figure 2 correspond to twice the standard deviation in the excitation interval 500-540 nm for EoY and 535-555 nm for PhB. The remaining decrease has to be attributed to mechanisms other than reabsorption and reemission, namely static quenching due to the absorption of aggregates or virtual traps and to dynamic quenching produced by excitation energy migration to those entities (29).

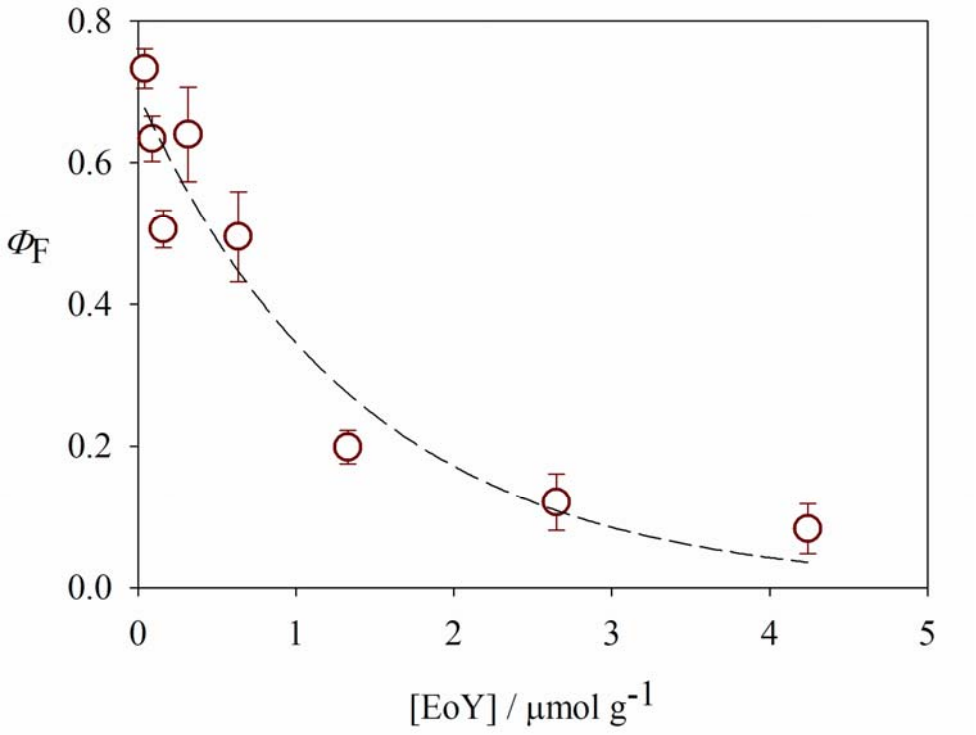
0.8
0.6
0.4
0.2
0.0
Φ_F
0
1
2
3
4
5
[EoY] / μmol g^{-1}

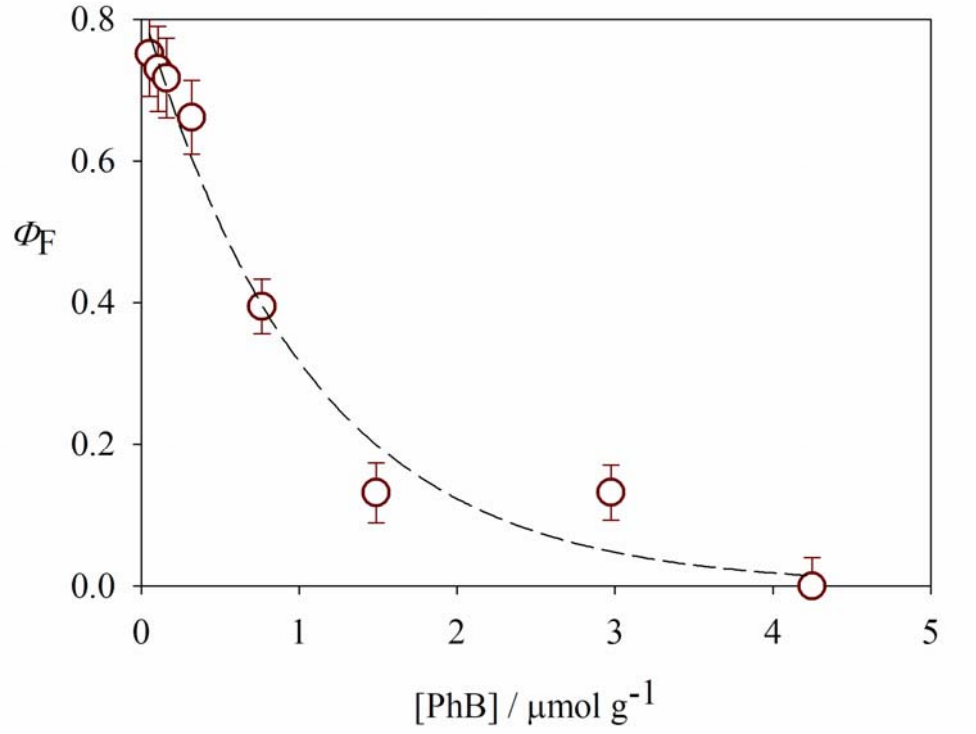
0.8
0.6
0.4
0.2
0.0
Φ_F
0
1
2
3
4
5
[PhB] / μmol g^{-1}

Figure 2. Corrected fluorescence quantum yields as a function of dye concentration for EoY (upper panel) and PhB (lower panel). See text for the meaning of error bars. Broken lines are exponential fitting functions without any physical meaning (see text).

Absolute triplet quantum yields obtained by LIOAS, $\Phi_{T,obs}$, are given in the SI (Table S3) for both dyes as a function of dye concentration together with values corrected by reabsorption of fluorescence using Eq. 2, Φ_T. As expected from Eq. 2, Φ_T is lower than $\Phi_{T,obs}$. The difference is greater at the lowest concentrations and its absolute value seldom exceeds 20 %, vanishing at the highest concentrations. Φ_T values are also displayed in Figure 3 together with those obtained by DRLFP and LIL, scaled to match values obtained by LIOAS. Before discussing the observed trends, DRLFP and LIL measurements will be addressed.

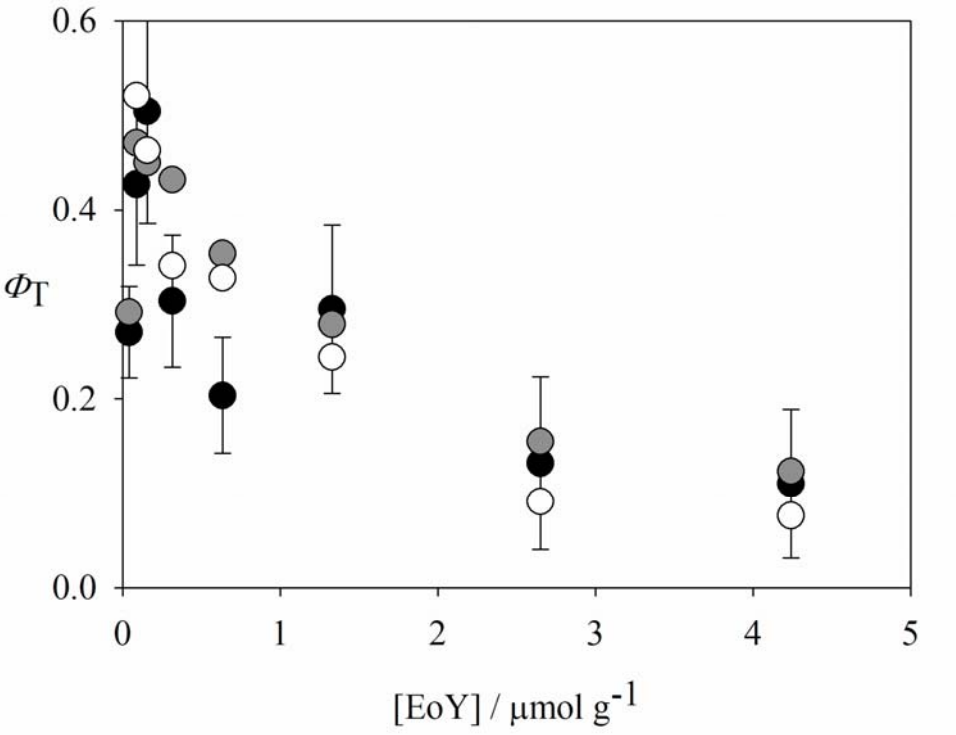
0.6
0.4
0.2
0.0
Φ_T
0
1
2
3
4
5
[EoY] / μmol g^{-1}

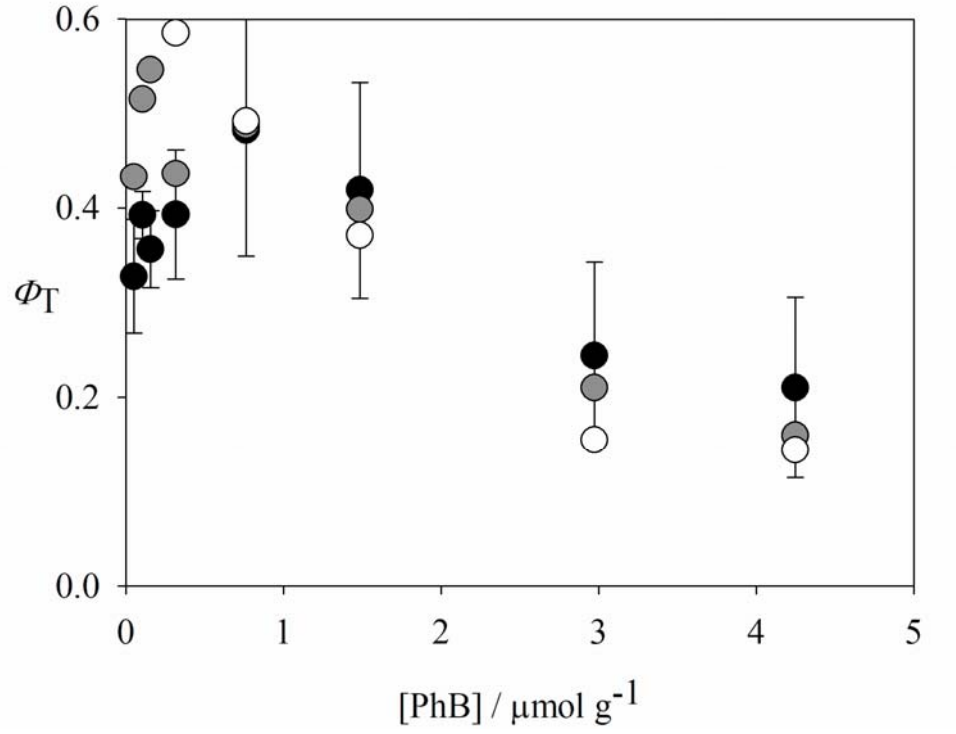
0.6
0.4
0.2
0.0
Φ_T
0
1
2
3
4
5
[PhB] / μmol g^{-1}

Figure 3. Corrected triplet quantum yields as a function of dye concentration for EoY (upper panel) and PhB (lower panel). Black circles correspond to LIOAS absolute determinations, while grey and white circles refer to scaled DRLFP and LIL relative determinations, respectively. Error bars for LIOAS data arise from 4 independent measurements.

Figure 4 shows the DRLFP signals obtained for EoY (upper panel) and PhB (lower panel). For both dyes, decays are independent of dye concentration. DRLFP and LIL signals are compared in the corresponding figure insets. The coincidence between DRLFP and LIL decays demonstrates that the species followed by DRLFP is effectively the triplet state for both dyes. In the case of EoY, both signals are analyzed at the same wavelength (680 nm) and, therefore, the DRLFP signal may be contaminated with some phosphorescence. However, this fact does not constitute any error source as both signals decay in the same way. On the contrary, for PhB phosphorescence is negligible at the analysis wavelength of DRLFP (610 nm).

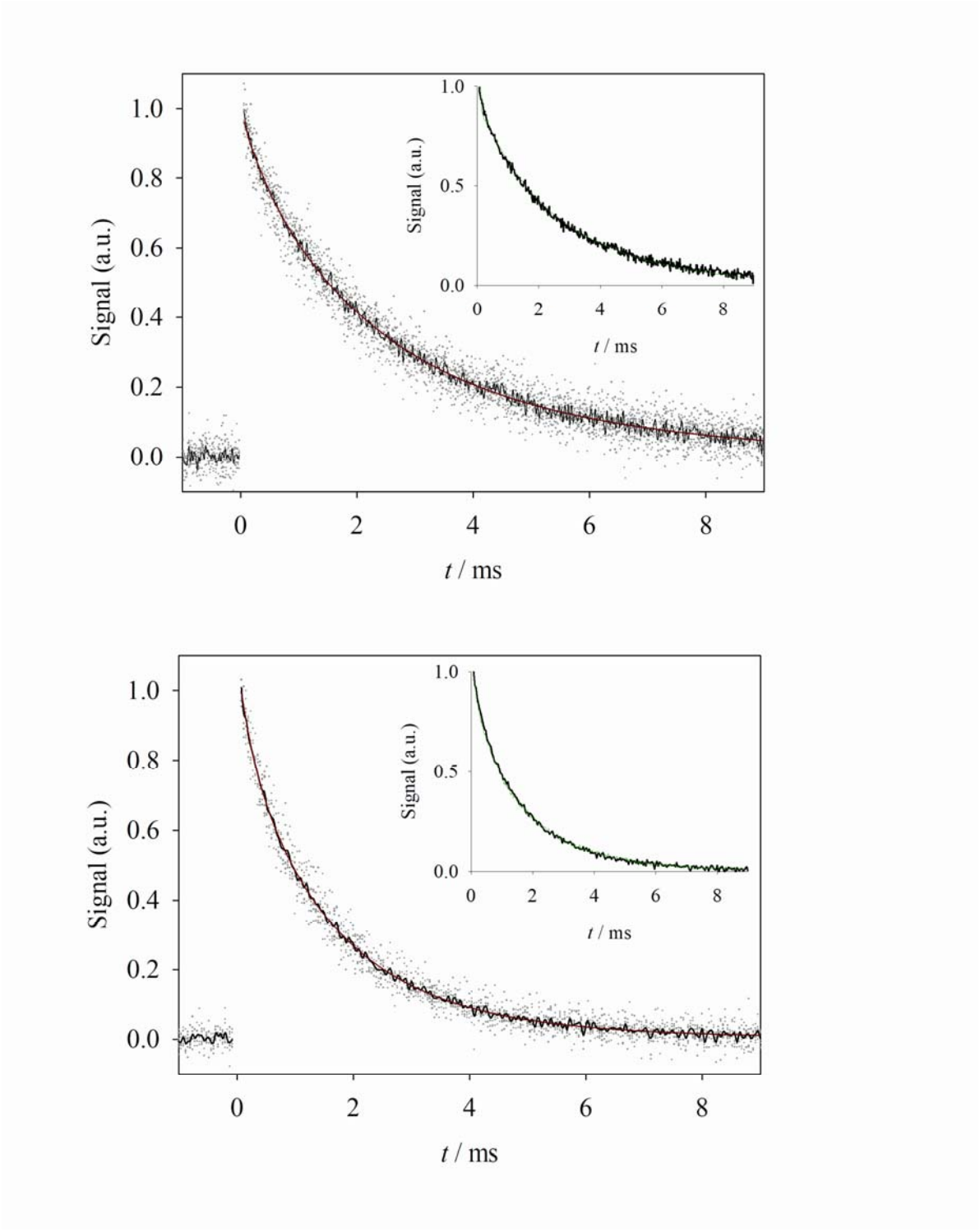
Signal (a.u.)
1.0
0.8
0.6
0.4
0.2
0.0
0
2
4
6
8
t / ms
Signal (a.u.)
1.0
0.5
0.0
0
2
4
6
8
t / ms
Signal (a.u.)
1.0
0.8
0.6
0.4
0.2
0.0
0
2
4
6
8
t / ms
Signal (a.u.)
1.0
0.5
0.0
0
2
4
6
8
t / ms

Figure 4. DRLFP decays for EoY (upper panel) and PhB (lower panel), for all samples (gray points scatter), average (black line) and triexponential fit (red line). Insets: DRLFP average (black) and LIL average (green). For EoY, both decays are analyzed at 680 nm, while for PhB DRLFP decays are analyzed at 610 nm and LIL decays at 695 nm.

The average of DRLFP and LIL signals normalized to unity at $t = 0$ can be fitted for EoY by a triexponential function: Signal = 0.08 exp(–t/0.30 ms) + 0.43 exp(–t/1.62 ms) + 0.49 exp(–t/3.80 ms). A more detailed study on the triplet decay was performed earlier (18), reporting a bimodal lifetime distribution with maxima peaking at ca. 0.75 and 3.00 ms. Similar results were obtained for PhB (see Figure 4, lower panel), with average DRLFP and LIL signals fitted also by a triexponential function: Signal = 0.19 exp(–t/0.25 ms) + 0.71 exp(–t/1.52 ms) + 0.10 exp(–t/3.70 ms). A bimodal triplet lifetime distribution with maxima peaking at ca. 0.5 and 1.8 ms was reported earlier for PhB included in microcrystalline cellulose (19). In both cases, the complex behavior of triplet decays was attributed to dye triplets sensing two different environments of cellulose, i.e., crystalline and amorphous. These facts demonstrate that triexponential decays are only an approximation for a more complex situation.

The DRLFP signals extrapolated to $t = 0$ were plotted as a function of the laser pulse energy (as an example see Figure S5 in the SI). Relative $\Phi_{T,obs}$ were calculated from the slope at the origin of these plots divided by the fraction of excitation light absorbed by the sample (see Materials and Methods). LIL signals could be measured accurately at lower laser pulse energies (< 50 μJ) and the slope at the origin was calculated from linear fittings. DRLFP measurements were noisier, and the number of points in the low-energy linear regime scarce, so that slopes were calculated using the fitting hyperbolic equation: signal($t = 0$) = aE/(b + E) + cE, where E is

the laser pulse energy. This fitting equation has no physical meaning; however, it was demonstrated in a previous work that it is a good extrapolation function (26).

Relative triplet quantum yields obtained from DRLFP and LIL measurements follow the same trend on increasing dye concentration, within the experimental error, compared with the absolute triplet quantum yields obtained from LIOAS (see Figure 3). This fact demonstrates that LIOAS signals arise in fact from the triplet state and confirms the concentration dependence found for Φ_T.

The trends in Φ_F and Φ_T with dye concentration are compared in Figure 5. The decrease of Φ_F with concentration is steeper than the decrease of Φ_T, being the difference more evident for PhB. Energy traps (dye aggregates and/or virtual statistical traps), which are responsible for fluorescence CQ, are at the same time an unexpected source of triplet states. This behavior will be explained in what follows.

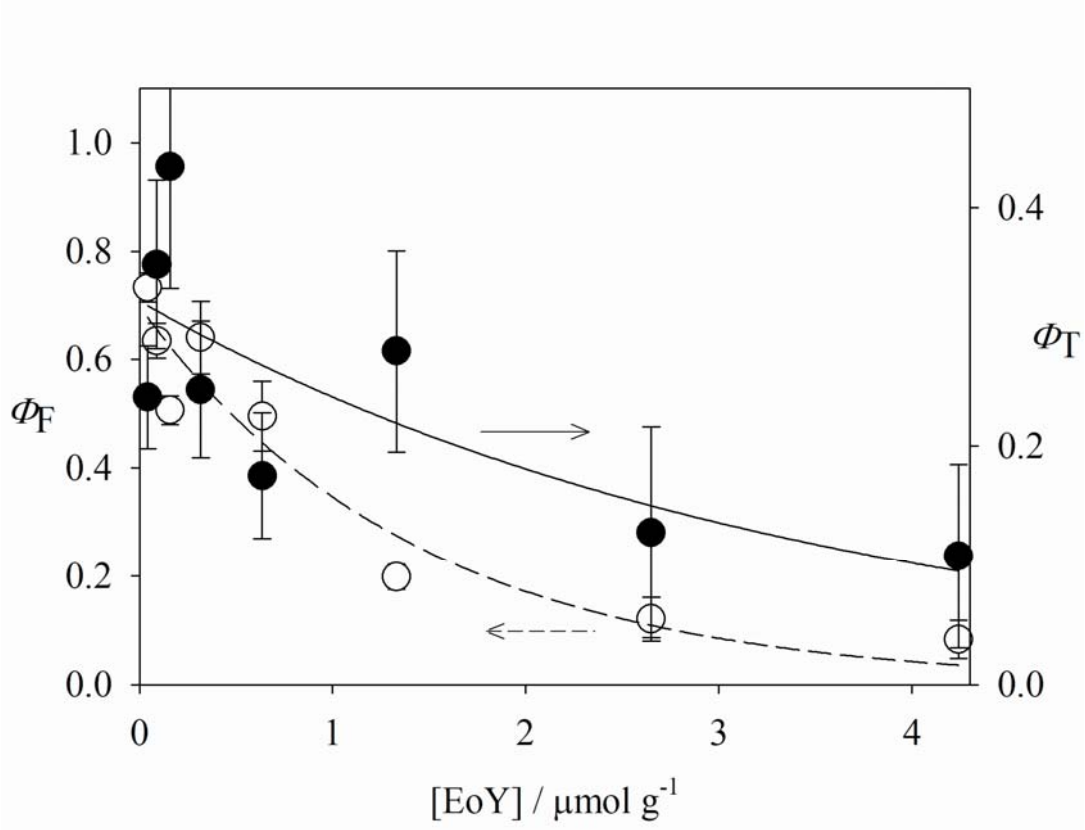
1.0
0.8
0.6
0.4
0.2
0.0
Φ_F
0.4
0.2
0.0
Φ_T
0
1
2
3
4
[EoY] / μmol g^{-1}

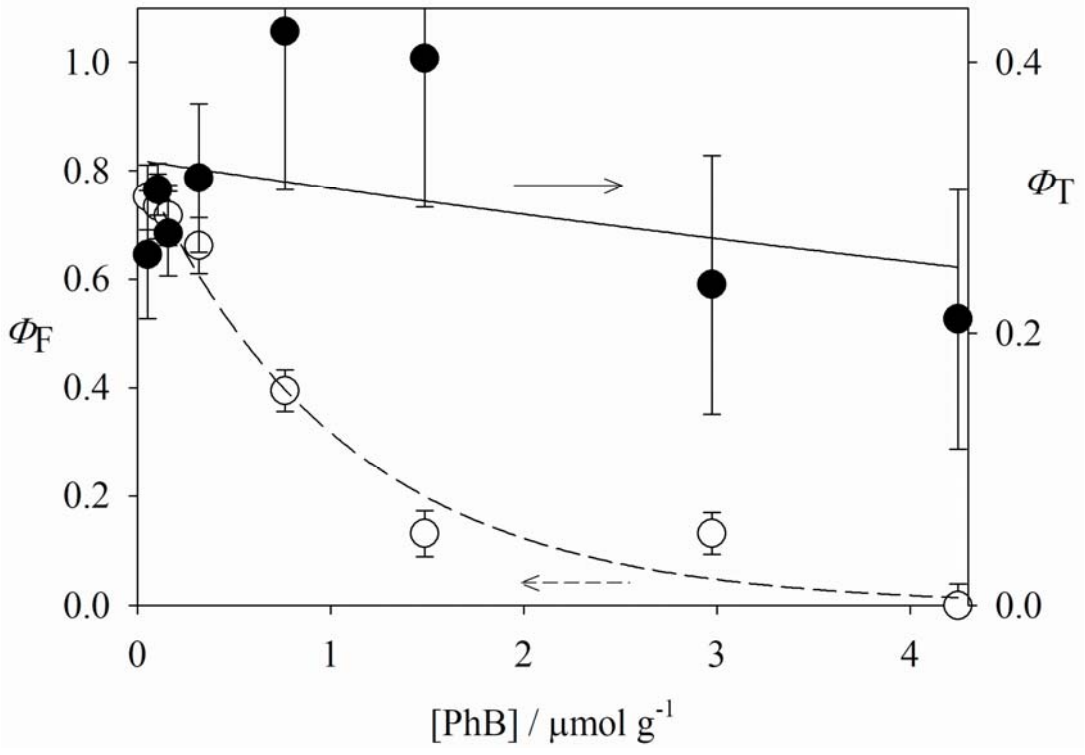
1.0
0.8
0.6
0.4
0.2
0.0
Φ_F
0.4
0.2
0.0
Φ_T
0
1
2
3
4
[PhB] / μmol g^{-1}

Figure 5. Effect of concentration on Φ_F and Φ_T for EoY (upper panel) and PhB (lower panel). Full lines are exponential fittings for Φ_T and broken lines are exponential fittings for Φ_F shown in Figure 2. These fittings have no physical meaning and are given only for comparison of the effect of concentration on quantum yields.

Fluorescence quenching on aggregation followed by triplet formation may be evaluated considering the exciton theory (31). In the strong coupling limit, exciton splitting in H-type aggregates leaves an optically allowed upper singlet excited state and a forbidden lower one. After excitation to the upper exciton state, rapid internal conversion takes place to the lower exciton state, thus preventing aggregate fluorescence. If the latter state is higher in energy than the triplet state of the dye, then triplet formation would be a possible deactivation pathway, favored by a reduction in the singlet-triplet energy gap. However, absorption spectroscopic results are consistent with weak or intermediate coupling, as slight spectral changes are observed for EoY on increasing concentration, while only small changes in band ratio and hypochromism are observed for PhB (32). As more significant spectroscopic changes would be expected in the case of strong coupling, particularly blue-shifts for H-type aggregates, exciton theory is not able to explain the observed behavior.

In a previous work on PhB included into microcrystalline cellulose (19), negligible changes in fluorescence lifetimes were observed on increasing dye concentration. An explanation of fluorescence quenching with triplet formation in the traps as a result of relative changes in radiative and non-radiative deactivation rate constants is not plausible because, in that case, changes in fluorescence lifetimes would have been expected on increasing dye concentration. Thus, it is reasonable to consider the presence of a new non-fluorescent excited state in the traps,

populated *via* a very efficient pathway from the singlet excited state, capable of yielding the triplet state at the expense of fluorescence and eventually internal conversion.

As mentioned in the Introduction, under appropriate conditions triplet formation may result from charge recombination of geminate radical anion – radical cation pairs formed *via* electron transfer from close lying excited molecules. The short distances in molecular aggregates or virtual traps favor electron transfer, insofar the energy of the charge-transfer (CT) state lies below the energy of the dye pair excited singlet. Thus, a radical pair recombination mechanism involving charge transfer quenching of the singlet state by neighboring dye molecules with subsequent spin flip may account for the observed behavior. A similar mechanism explains the formation of the P680 triplet state in the reaction center of PSII (13). The CT state should be more energetic than the dye pair triplet state. The postulated mechanism is shown in Scheme I.

Scheme I. Proposed mechanism of triplet formation in dimeric traps (M: monomer).

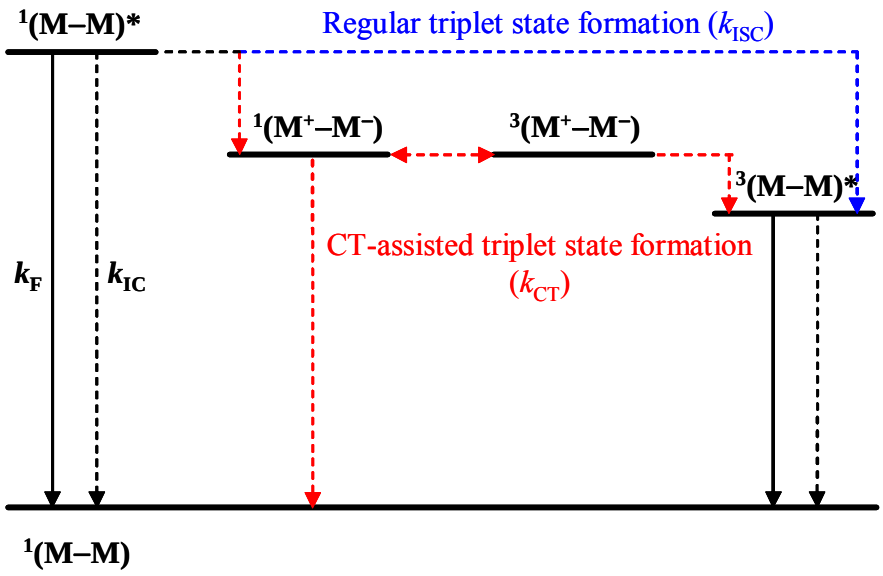

The singlet excited state of the pair ^{1}(M–M)*, produced by direct light absorption or energy transfer from dye monomers, undergoes rapid charge transfer with the formation of a radical anion – radical cation pair in the singlet state $^1(M^+–M^–)$. Spin-orbit coupling leads to the triplet state $^3(M^+–M^–)$. The energy of the singlet and triplet radical ion pairs may be similar due to negligible spin correlation. As an example, according to experimental results and calculations in electron donor (D) – bridge – acceptor (A) dyads, at D-A separations between 1 to 1.5 nm, this energy gap is in the order of a few cm^{-1} and a rapid interconversion between $^1(M^+–M^–)$ and $^3(M^+–M^–)$ is expected (33). Charge recombination in $^3(M^+–M^–)$ leads to the pair triplet state ^{3}(M–M)* under appropriate energetic conditions. Additionally, ^{3}(M–M)* may be formed directly from ^{1}(M–M)* (regular triplet state formation, see Scheme I). As excitonic interactions depend on the square of the transition moment, negligible for triplet dye pairs, the pair behaves as an isolated, monomeric triplet, decaying therefore with the same lifetime as ^{3}M.

In order to test the feasibility of the CT-assisted mechanism, the energetics of the dye radical ion pair is considered through the estimation of the standard Gibbs energy of photoinduced electron transfer (34):

$$\Delta_{\mathrm{ET}}G^0 = N_A\left\{e\left[E^0(\mathrm{D}^{+\bullet}/\mathrm{D}) - E^0(\mathrm{A}/\mathrm{A}^{-\bullet})\right] + w(\mathrm{D}^{+\bullet}\mathrm{A}^{-\bullet}) - w(\mathrm{DA})\right\} - \Delta E_{0,0} = E_{\mathrm{CT}} - \Delta E_{0,0} \qquad (3)$$

where e is the elementary charge, N_A is the Avogadro constant, $E^0(D^{+\bullet}/D)$ and $E^0(A/A^{-\bullet})$ are the redox potentials of the dye acting as electron donor and acceptor, respectively (both relative to the same reference electrode), $\Delta E_{0,0}$ is the vibrational zero electronic energy of the excited dye, and $w(D^{+\bullet}\ A^{-\bullet})$ and w(DA) are electrostatic work terms, calculated as:

$$\begin{aligned} w(\mathrm{D}^{+\bullet}\mathrm{A}^{-\bullet}) &= z(\mathrm{D}^{+\bullet})\, z(\mathrm{A}^{-\bullet})\, e^2 / (4\pi\, \varepsilon_0\, \varepsilon_r\, a) \\ w(\mathrm{DA}) &= z(\mathrm{D})\, z(\mathrm{A})\, e^2 / (4\pi\, \varepsilon_0\, \varepsilon_r\, a) \end{aligned} \qquad (4)$$

where z(X) is the charge of species X, a is the distance between dyes within the pair, ε_0 is the vacuum permittivity and ε_r is the relative medium static permittivity. From Eq~~n~~. (3) the energy of the radical ionic pair, E_{CT}, is calculated. Relevant parameters and estimations are shown in Table 1. $\Delta E_{0,0}$ was estimated by computing the lowest excited singlet energies (E_S) from the cross point of normalized absorption and emission spectra, thus disregarding any entropic contribution (35). The triplet energies (E_T) were estimated from phosphorescence maxima reported in cellulose (18,19). The value of ε_r for cellulose was approximated as that in methanol.

Table 1. Relevant parameters and estimations for photoinduced electron transfer.

	$E^0(D^{+\bullet}/D)$ / V	$E^0(A/A^{-\bullet})$ / V	E_S / eV	E_T / eV	$\Delta_{ET}G^0$ / eV	E_{CT} / eV [3]
Eosin Y[1]	0.76	-1.09	2.29	1.77	-0.48	1.81
Phloxine B[2]	(0.90)	(-0.99)	2.22	1.70	-0.37	1.85
Rose Bengal[2]	0.90	-0.99	2.18	1.68	-0.33	1.85

[1] Redox potentials in methanol (vs Ag/AgCl) (36).

[2] Redox potentials in methanol (vs Ag/AgCl) estimated for PhB from values reported for Rose Bengal (RB) (37,38).

[3] Calculated considering a distance of 1 nm between molecules within the trap and the permittivity of methanol.

Photoinduced electron transfer within close lying dye molecules is a thermodynamically allowed process for both EoY and PhB, assuming redox potentials for RB apply to PhB (see Table 1). In both cases the energy of the charge transfer state lies above the energy of the dye triplet state (E_T), fulfilling the energetic conditions for CT-assisted triplet formation.

Photoinduced electron transfer could be a very fast process (sub-nanosecond time scale) at the molecular distances within an aggregate or virtual trap (< 1.5 nm), competitive with or even faster than fluorescence decays in the ns range, thus resulting in fluorescence quenching (39–40). The energy gap estimated between $^1(M–M)^*$ and $^1(M^+–M^-)$ is ca. 0.5 eV for both dyes. Typical total reorganization energies for molecular dyads in organic solvents, comprising molecules with π-extended systems such as porphyrins, are about 1 eV (41,42). Similar values were obtained for charge transfer reactions in proteins (43), whereas smaller values were reported for fullerene-containing dyads (44). According to the estimated driving force, in our case charge separation is expected to be in the normal Marcus region and probably not so far from the optimal conditions, thus leading to fast singlet state deactivation (45). Charge recombination to the ground state is expected to be in the sub-μs time scale due to the large value of E_{CT} ca. 1.8 eV, being most probably in the inverted Marcus region (46). On the other hand, the energy gap for charge recombination in the triplet state is estimated as 0.04 eV for EoY and 0.15 eV for PhB (see Table 1), which lies in the normal Marcus region but far from the optimal conditions. Thus, triplet formation by traps would result from the competition between the different charge-recombination pathways of the intermediate CT state. Back electron transfer from the triplet to the CT state is probably precluded by a kinetic barrier, as no changes in triplet lifetimes were observed on increasing concentration for both dyes. These arguments demonstrate the feasibility of the proposed mechanism. Aside from the example in photosynthesis mentioned above, similar mechanisms have also been proposed for several molecular dyads (15,33,44,47,48) and even for conjugated polymer aggregates (49).

According to Scheme I and neglecting charge recombination to the ground state, the fluorescence and triplet state quantum yields for dimeric traps can be expressed as:

$$\Phi_{\mathrm{Fd}} = \frac{k_{\mathrm{F}}}{k_{\mathrm{F}} + k_{\mathrm{IC}} + k_{\mathrm{ISC}} + k_{\mathrm{CT}}} \tag{5}$$

$$\Phi_{\mathrm{Td}} = \frac{k_{\mathrm{ISC}} + k_{\mathrm{CT}}}{k_{\mathrm{F}} + k_{\mathrm{IC}} + k_{\mathrm{ISC}} + k_{\mathrm{CT}}} \tag{6}$$

where k_F and k_{IC} have the usual meaning, k_{ISC} is the rate constant for regular triplet state formation, and k_{CT} is the overall rate constant for CT-assisted triplet state formation. It is clear from Eqs. (5) and (6) that, assuming that k_F, k_{IC} and k_{ISC} are the same for dye monomers and dimeric traps, Φ_F will be lower and Φ_T will be higher as the concentration of traps increases. However, our experience involving different dyes in various solid environments shows that, as dye concentration further increases, oligomeric traps are formed, leading finally to extinction of fluorescence and triplet formation.

Triplet formation by dye aggregates was previously suggested for RB included in microcrystalline cellulose (26) and confirmed for the same dye included in poly(2-hydroxyethyl methacrylate) (pHEMA) thin films (4). In both cases, fluorescent dimers capable of rendering triplet states were observed, whereas higher-order aggregates were dark and photochemically inactive. Fluorescence and triplet (or singlet oxygen) quantum yields followed similar trends on increasing dye concentration, with a slightly different ratio between fluorescence and singlet oxygen quantum yields for monomers and dimers. Fluorescent dimers were also observed earlier for RB included in cellulose (28). However, in spite of these results, a situation similar to that shown in Fig. 5 was never observed for RB, though estimations in Table 1 predicts CT-assisted triplet state formation also in this case. A possible explanation is as follows. The presence of iodine in the RB structure is responsible for a high Φ_T value, leading to low fluorescence quantum yields – Φ_F = 0.09 in methanol (36), 0.018 in water (50), 0.12 in cellulose (28) and 0.05 in pHEMA (4) – and short fluorescence lifetimes – τ_F = 0.6 ns in methanol and 0.095 ns in water

(36, 50) –. Therefore, it is expected that k_{CT} has a low weight in Eqs. (5) and (6). If this is the case, $\Phi_F / \Phi_T \approx k_F / k_{ISC}$ would be similar for monomers and dimeric traps. Fluorescence lifetimes in ethanol are substantially longer for EoY, 3.47 ns (30), and PhB, 3.65 ns (51), therefore allowing fluorescence quenching by charge transfer.

According to the proposed mechanism, the photophysics of dye traps depends on the energy of the CT intermediate state and the fluorescence lifetime. The energy depends in turn on the environment (mainly through the medium permittivity). Thus, changes in the supporting material may have strong influence on the photophysical behavior. Recently, we studied the photophysics of PhB included in pHEMA thin films as a function of dye concentration (3). Fluorescence and singlet oxygen quantum yields follow the same trend on increasing dye concentration. This behavior contrasts with the evidence found in cellulose. If the same mechanism is still operative, the change in molecular environment may be responsible for charge-transfer state stabilization below the triplet level, thus precluding triplet formation by PhB traps in pHEMA. On the contrary, changes in the molecular environment are not expected to have major influence on RB dimeric traps because, as mentioned earlier, the CT-assisted mechanism should not be relevant as a deactivation pathway in this case, irrespective of the supporting material (cellulose or pHEMA).

Conclusions

Interactions resulting from molecular crowding at high concentrations lead generally to energy trapping, this being one of the main factors in lowering the efficiency of heterogeneous photosensitizers. The formation of dye aggregates or virtual traps is responsible for fluorescence quenching. In this work we demonstrate that energy traps may lead to the formation of dye triplet

states at concentrations at which fluorescence is already almost extinguished. A mechanism including the intermediacy of CT states within the trap is proposed and calculations demonstrate its feasibility. The capability of traps to produce triplet states results from the balance between the energies of the excited states and the intermediate CT states, which strongly depends on molecular structure, intermolecular distances and the environment. On the other hand, the formation of spectroscopically evidenced ground-state molecular aggregates (dimers and/or oligomers) may open new non-radiative deactivation pathways competing with charge transfer or intersystem crossing, leading to the formation of inactive traps. The control over the deactivation pathways that regulate the photophysical behavior of dye aggregates requires tuning redox potentials, intermolecular distances and eventually orientations within the aggregates. The present work demonstrates that photoactive energy traps, capable of producing triplet states of the dye, can be formed even in highly-concentrated systems with dyes distributed at random. This may configure a strategy to surpass limitations posed by concentration quenching in various applications, including photosensitization and photocatalysis.

Acknowledgements

This work has been supported by the University of Buenos Aires, the National Research Council of Argentina (CONICET) and the Agencia Nacional de Promoción Científica y Tecnológica (ANPCyT). H. B. R. and E. S. R. are members of CONICET. Y. L. held a fellowship from the Consejo Interuniversitario de Rectores (CIN).

Supporting Information

Additional Supporting Information may be found in the online version of this article: Spectroscopic data, observed and corrected fluorescence and triplet quantum yields, and DRLFP signals.

References

1. López, S. G., G. Worringer, H. B. Rodríguez and E. San Román (2010) Trapping of Rhodamine 6G excitation energy on cellulose microparticles. *Phys. Chem. Chem. Phys.* **12**, 2246-2253.

2. Beddard, G. S. and G. Porter (1976) Concentration quenching in chlorophyll. *Nature* **260**, 366-367.

3. Litman, Y., H. B. Rodríguez and E. San Román (2016) Tuning the concentration of dye loaded polymer films for maximum photosensitization efficiency: phloxine B in poly(2-hydroxyethyl methacrylate). *Photochem. Photobiol. Sci.* **15**, 80-85.

4. Ezquerra Riega, S. D., H. B. Rodríguez and E. San Román (2017) Rose bengal in poly(2-hydroxyethyl methacrylate) thin films: self-quenching by photoactive energy traps. *Methods Appl. Fluoresc.* **5**, 014010, DOI: 10.1088/2050-6120/aa61ae.

5. Rabinowitch, E. I. (1951) *Photosynthesis and Related Processes*, Vol. II, Part 1, Interscience, pp. 759ff.

6. Birks, J. B. (1970) *Photophysics of Aromatic Molecules*, Wiley, London.

7. Mei, J., N. L. C. Leung, R. T. K. Kwok, J, W. Y. Lam and B. Z. Tang (2015) Aggregation-induced emission: Together we shine, united we soar! *Chem. Rev.* **115**, 11718-11940.

8. Dong, Y. (2013) Crystallization-induced emission enhancement. In Aggregation-Induced Emission: Fundamentals (Edited by Z. Tang and A. Qin), pp. 323-336. John Wiley & Sons, Ltd., West Sussex.

9. Lucenti, E., A. Forni, C. Botta, L. Carlucci, C. Giannini, D. Marinotto, A. Previtali, S. Righetto and E. Cariati (2017) H-aggregates granting crystallization-induced emissive behavior and ultralong phosphorescence from a pure organic molecule. *J. Chem. Phys. Lett.* **8**, 1894-1898.

10. Yang, L., X. Wang, G. Zhang, X. Chen, G. Zhang and J. Jiang (2016) Aggregation-induced intersystem crossing: A novel strategy for efficient molecular phosphorescence. *Nanoscale* **8,** 17422-17426.

11. Hong, Y. (2016) Aggregation-induced emission-fluorophores and applications. *Methods Appl. Fluoresc.* **4**, 022003, **DOI:** 10.1088/2050-6120/4/2/022003.

12. Lopez, S. G., L. Crovetto, J. M. Alvarez-Pez, E. M. Talavera and E. San Román (2014) Fluorescence enhancement of a fluorescein derivative upon adsorption on cellulose. *Photochem. Photobiol. Sci.* **13**, 1311-1320.

13. Booth, P. J., B. Crystall, L. B. Giorgi, J. Barber, D. R. Klug and G. Porter (1990) Thermodynamic properties of D1/D2/cytochrome b-559 reaction centres investigated by time-resolved fluorescence measurements. *Biochim. Biophys. Acta* **1016**, 141-152.

14. Filatov, M. A., S. Karuthedath, P. M. Polestshuk, H. Savoie, K. J. Flanagan, C. Sy, E. Sitte, M. Telitchko, F. Laquai, R. W. Boyle and M. O. Senge (2017) Generation of triplet excited states via photoinduced electron transfer in meso-anthra-BODIPY: Fluorogenic response toward singlet oxygen in solution and in vitro. *J. Am. Chem. Soc.* **139**, 6282-6285.

15. Kim, Y. Zhou, N. Tohnai, H. Nakatsuji, M. Matsusaki, M. Fujitsuka, M. Miyata and T. Majima (2018) Aggregation-induced singlet oxygen generation: functional fluorophore and anthrylphenylene dyad self-assemblies. *Chem. An Eur. J.* **24**, 636-645.

16. Williams, R. M., H. C. Chen, D. D. Nuzzo, S. C. J. Meskers and R. A. J. Janssen (2017) Ultrafast charge and triplet state formation in diketopyrrolopyrrole low band gap polymer/fullerene blends: influence of nanoscale morphology of organic photovoltaic materials on charge recombination to the triplet state. *J. Spectrosc.* Article ID 6867507.

17. Rao, A., P. C. Y. Chow, S. Gélinas, C. W. Schlenker, C. Z. Li, H. L. Yip, A. K. Y. Jen, D. S. Ginger and R. H. Friend. (2013) The role of spin in the kinetic control of recombination in organic photovoltaics. *Nature* **500**, 435-439.

18. Rodríguez, H. B., E. San Román, P. Duarte, I. Ferreira Machado and L. F. Vieira Ferreira (2012) Eosin Y triplet state as a probe of spatial heterogeneity in microcrystalline cellulose. *Photochem. Photobiol.* **88**, 831-839.

19. Duarte P., D. P. Ferreira, I. Ferreira Machado, L. F. Vieira Ferreira, H. B. Rodríguez and E. San Román (2012) Phloxine B as a probe for entrapment in microcrystalline cellulose. *Molecules* **17**, 1602-1616.

20. Wilkinson, F., P. A. Leicester, L. F. Vieira Ferreira and V. M. M. R. Freire (1991) Photochemistry on surfaces: triplet-triplet energy transfer on microcrystalline cellulose studied by diffuse reflectance transient absorption and emission spectroscopy. *Photochem. Photobiol.* **54**, 599-608.

21. Mirenda, M., M. G. Lagorio and E. San Román (2004) Photophysics on Surfaces: Determination of Absolute Fluorescence Quantum Yields from Reflectance Spectra. *Langmuir* **20**, 3690-3697.

22. Wendlandt, W. W. and H. G. Hecht (1966) *Reflectance Spectroscopy*, Ch. 3, pp. 55-76. Wiley Interscience, New York, NY.

23. Tomasini, E. P., S. E. Braslavsky and E. San Román (2012) Triplet Quantum Yields in Light-Scattering Powder Samples Measured by Laser-Induced Optoacoustic Spectroscopy (LIOAS). *Photochem. Photobiol. Sci.* **11**, 1010-1017.

24. Tomasini, E. P., E. San Román and S. E. Braslavsky (2009) Validation of Fluorescence Quantum Yields for Light-Scattering Powdered Samples by Laser-Induced Optoacoustic Spectroscopy. *Langmuir* **25**, 5861-5868.

25. Kessler, R. W., G. Krabichler, S. Uhl, D. Oelkrug, W. P. Hagan, J. Hyslop and F. Wilkinson (1983) Transient decay following pulse excitation of diffuse scattering samples. *Optica Acta* **8**, 1099-1111.

26. Litman, Y., M. G. Voss, H. B. Rodríguez and E. San Román (2014) Effect of concentration on the formation of rose bengal triplet state on microcrystalline cellulose: A combined laser-induced optoacoustic spectroscopy, diffuse reflectance flash photolysis and luminescence study. *J. Phys. Chem. A* **118**, 10531-10537.

27. Lagorio, M. G., L. E. Dicelio, M. I. Litter and E. San Román (1998) Modeling of fluorescence quantum yields of supported dyes. Aluminum carboxyphthalocyanine on cellulose. *J. Chem. Soc. Faraday Trans.* **94**, 419-425.

28. Rodríguez, H. B., M. G. Lagorio and E. San Román (2004) Rose bengal adsorbed on microgranular cellulose: Evidence on fluorescent dimers. *Photochem. Photobiol. Sci.* **3**, 674-680.

29. Rodríguez, H. B. and E. San Román (2013) Effect of Concentration on the Photophysics of Dyes in Light Scattering Materials. *Photochem. Photobiol.* **89**, 1273-1282.

30. Zhang, X. –F., J. Zhang and L. Liu (2014) Fluorescence Properties of Twenty Fluorescein derivatives: Lifetime, quantum yield, absorption and emission spectra. *J. Fluoresc.* **24**, 819-826.

31. Kasha, M., H. R. Rawls and M. Ashraf El-Bayoumi (1965) The Exciton Model in Molecular Spectroscopy. *Pure Appl. Chem.* **2**, 371-391.

32. Kasha, M. (1963) Energy Transfer Mechanism and The Molecular Exciton Model for Molecular Aggregates. *Radiat. Res.* **20**, 55-71.

33. Verhoeven, J. W. (2006) On the role of spin correlation in the formation, decay and detection of long-lived, intramolecular charge-transfer states. *J. Photochem. Photobiol. C* **7**, 40-60.

34. Braslavsky, S. E. (2007) Glossary of Terms used in Photochemistry. 3rd Edition. *Pure Appl. Chem.* **79**, 293-465.

35. Suppan, P. and E. Vauthey (1989) The Energy Balance of Photoinduced Electron Transfer Reactions. *J. Photochem. Photobiol. A* **49**, 239-248.

36. Zhang, X. –F., I. Zhang and L. Liu (2010) Photophysics of Halogenated Fluoresceins: Involvement of Both Intramolecular Electron Transfer and Heavy Atom Effect in the Deactivation of Excited States. *Photochem. Photobiol.* **86**, 492-498.

37. Linden, S. M. and D. C. Neckers (1988) Bleaching Studies of Rose Bengal Onium Salts. *J. Am. Chem. Soc.* **110**, 1257-1260.

38. Lee, S. H., D. H. Nam and C. B. Park (2009) Screening Xanthene Dyes for Visible Light-Driven Nicotinamide Adenine Dinucleotide Regeneration and Photoenzymatic Synthesis. *Adv. Synth. Catal.* **351**, 2589-2594.

39. Miller, J. R., J. A. Peeples, M. J. Schmitt and G. L. Closs (1982) Long-Distance Fluorescence Quenching by Electron Transfer in Rigid Solutions. *J. Am. Chem. Soc.* **104**, 6488-6493.

40. Miller, J. R., L. T. Calcaterra and G. L. Closs (1984) Intramolecular Long-Distance Electron Transfer in Radical Anions. The Effects of Free Energy and Solvent on the Reaction Rates. *J. Am. Chem. Soc.* **106**, 3047-3049.

41. Osuka, A., G. Noya, S. Taniguchi, T. Okada, Y. Nishimura, I. Yamazaki and N. Mataga (2000) Energy-Gap Dependence of Photoinduced Charge Separation and Subsequent Charge Recombination in 1,4-Phenylene-Bridged Zinc-Free-Base Hybrid Porphyrins. *Chem. Eur. J.* **6**, 33-46.

42. DeGraziano, J. M., P. A. Liddell, L. Leggett, A. L. Moore, T. A. Moore and D. Gust (1994) Free Energy Dependence of Photoinduced Charge Separation Rates in Porphyrin Dyads. *J. Phys. Chem.* **98**, 1758-1761.

43. Krishtalik, L. I. (2011) The medium reorganization energy for the charge transfer reactions in proteins. *Biochim. Biophys. Acta* **1807**, 1444-1456.

44. Ohkubo, K., H. Imahori, J. Shao, Z. Ou, K. M. Kadish, Y. Chen, G. Zheng, R. K. Pandey, M. Fujitsuka, O. Ito and S. Fukuzumi (2002) Small Reorganization Energy of Intramolecular Electron Transfer in Fullerene-Based Dyads with Short Linkage. *J. Phys. Chem. A* **106**, 10991-10998.

45. Marcus, R. A. (1993) Electron transfer reactions in chemistry. Theory and experiment. *Rev. Mod. Phys.* **65**, 599-610.

46. Warman, J. M., K. J. Smit, M. P. de Haas, S. A. Jonker, M. N. Paddon-Row, A. M. Oliver, J. Kroon, H. Oevering and J. W. Verhoeven (1991) Long-Distance Charge Recombination within Rigid Molecular Assemblies in Nondipolar Solvents. *J. Phys. Chem.* **95**, 1979-1987.

47. Tran-Thi, T. H., J. F. Lipskier, P. Maillard, M. Momenteau, J.-M. Lopez-Castillo and J.-P. Jay-Gerin (1992) Effect of the Exciton Coupling on the Optical and Photophysical Properties of Face-to-Face Porphyrin Dimer and Trimer. A Treatment Including the Solvent Stabilization Effect. *J. Phys. Chem.* **96**, 1073-1082.

48. Veldman, D., S. M. A. Chopin, S. C. J. Meskers, M. M. Groeneveld, R. M. Williams and R. A. J. Janssen (2008) Triplet Formation Involving a Polar Transition State in a Well-Defined Intramolecular Perylenediimide Dimeric Aggregate. *J. Phys. Chem. A* **112**, 5846-5857.

49. Thomas, A. K, H. A. Brown, B. D. Datko, J. A. Garcia-Galvez and J. K. Grey (2016) Interchain Charge-Transfer States Mediate Triplet Formation in Purified Conjugated Polymer Aggregates. *J. Phys. Chem. C* **120**, 23230-23238.

50. Fleming, G. R., A. W. E. Knight, J. M. Morris, R. J. S. Morrison and G. W. Robinson (1977) Picosecond Fluorescence Studies of Xanthene Dyes. *J. Am. Chem. Soc.* **99**, 4306-4311.

51. Malak, H. (1999) Investigating up-conversion fluorescence of Phloxine B. *IEEE Eng. Med. Biol.* **99**, 37-91.